Comments p-PK

Check spelling consistency throughout e.g. centre, optimize etc

Eur. Phys. J. C manuscript No.
(will be inserted by the editor)

Search for the Lepton Flavour Violating Decay $\mu^+ \to e^+\gamma$ with the Full Dataset of the MEG experiment

A. M. Baldini [4a], Y. Bao [1], E. Baracchini [3,17], C. Bemporad [4ab], F. Berg [1,2], M. Biasotti [8ab], G. Boca [6ab], P. W. Cattaneo [*,6a], G. Cavoto [7a], F. Cei [4ab], C. Cerri [4a], G. Chiarello [13ab], C. Chiri [13ab], A. Corvaglia [13ab], A. de Bari [6ab], M. De Gerone [8a], T. Doke [†,9], A. D'Onofrio [4ab], S. Dussoni [4a], J. Egger [1], Y. Fujii [3], L. Galli [4a], F. Gatti [8ab], F. Grancagnolo [13a], M. Grassi [4a], A. Graziosi [7ab], D. N. Grigoriev [10,14,15], T. Haruyama [11], M. Hildebrandt [1], Z. Hodge [1,2], K. Ieki [3,1], F. Ignatov [10,15], T. Iwamoto [3], D. Kaneko [3], Tae Im Kang [5], P.-R. Kettle [1], B. I. Khazin [†,10,15], N. Khomutov [10], A. Korenchenko [12], N. Kravchuk [12], G. M. A. Lim [5], A. Maki [11], S. Mihara [11], W. Molzon [5], Toshinori Mori [3], F. Morsani [4a], A. Mtchedilishvili [1], D. Mzavia [†,12], S. Nakaura [3], R. Nardò [6ab], D. Nicolò [4ab], H. Nishiguchi [11], M. Nishimura [3], S. Ogawa [3], W. Ootani [3], S. Orito [†,3], M. Panareo [13ab], A. Papa [1], R. Pazzi [†,4], A. Pepino [13ab], G. Piredda [7a], G. Pizzigoni [8ab], A. Popov [10,15], F. Raffaelli [4a], F. Renga [1,7a], E. Ripiccini [7ab], S. Ritt [1], M. Rossella [6a], G. Rutar [1,2], R. Sawada [3], F. Sergiampietri [4a], G. Signorelli [4a], M. Simonetta [6ab], G. F. Tassielli [13a], F. Tenchini [4ab], Y. Uchiyama [3], M. Venturini [4a, 16], C. Voena [7a], A. Yamamoto [11], K. Yoshida [3], Z. You [5], Yu.V. Yudin [10,15], D. Zanello [7]

[1]Paul Scherrer Institut PSI, 5232, Villigen, Switzerland
[2]Swiss Federal Institute of Technology ETH, 8093 Zürich, Switzerland
[3]ICEPP, The University of Tokyo, 7-3-1 Hongo, Bunkyo-ku, Tokyo 113-0033, Japan
[4]INFN Sezione di Pisa[a]; Dipartimento di Fisica[b] dell'Università, Largo B. Pontecorvo 3, 56127 Pisa, Italy
[5]University of California, Irvine, CA 92697, USA
[6]INFN Sezione di Pavia[a]; Dipartimento di Fisica[b] dell'Università, Via Bassi 6, 27100 Pavia, Italy
[7]INFN Sezione di Roma[a]; Dipartimento di Fisica[b] dell'Università "Sapienza", Piazzale A. Moro, 00185 Roma, Italy
[8]INFN Sezione di Genova[a]; Dipartimento di Fisica[b] dell'Università, Via Dodecaneso 33, 16146 Genova, Italy
[9]Research Institute for Science and Engineering, Waseda University, 3-4-1 Okubo, Shinjuku-ku, Tokyo 169-8555, Japan
[10]Budker Institute of Nuclear Physics of Siberian Branch of Russian Academy of Sciences, 630090, Novosibirsk, Russia
[11]KEK, High Energy Accelerator Research Organization 1-1 Oho, Tsukuba, Ibaraki, 305-0801, Japan
[12]Joint Institute for Nuclear Research, 141980 Dubna, Russia
[13]INFN Sezione di Lecce[a]; Dipartimento di Matematica e Fisica[b] dell'Università, Via per Arnesano, 73100 Lecce, Italy
[14]Novosibirsk State Technical University, 630092 Novosibirsk, Russia
[15]Novosibirsk State University, 630090 Novosibirsk, Russia
[16]Scuola Normale Superiore, Piazza dei Cavalieri 7, 56126 Pisa, Italy
[17]*Present Address*: INFN, Laboratori Nazionali di Frascati, Via E. Fermi, 40-00044 Frascati, Rome, Italy

Received: date / Accepted: date

of the search ...

Abstract The analysis of the full dataset collected by the MEG experiment at the Paul Scherrer Institut in the period 2009–2013, totalling 7.5×10^{14} stopped muons on target, in the search for the lepton flavour violating decay $\mu^+ \to e^+\gamma$ is presented. A new upper limit on the branching ratio of this decay of 4.2×10^{-13} (90% confidence level) is established, which represents the most stringent limit on the existence of this decay to date.

Keywords Decays of muons, Lepton Flavor Violation, Flavour symmetries, Supersymmetry

*Corresponding author: paolo.cattaneo@pv.infn.it
†Deceased

Contents

1 Introduction

Section coordinator: P.W. Cattaneo
Text: 1.5
Figure: 2

The Standard Model (SM) allows Charged Lepton Flavour Violating (CLFV) processes only with minuscules branching ratios ($\ll 10^{-50}$) even accounting for neutrino masses and mixing. Therefore such decays, which are free by the theoretical uncertainties plaguing processes involving directly or indirectly hadronic states, are ideal laboratories for searching for new physics beyond the SM, which will be unambiguously signalled by the detection of such decays.

Existence of such decays at a measurable rate not far from current limits is suggested by many SM extensions such as supersymmetry [1] (an extensive review of the theoretical expectations on CLFV is provided in [2]). Hence, CLFV searches with improved sensitivity will probe new regions of the parameter space of SM extensions. The $\mu^+ \to e^+\gamma$ decay is particularly sensitive to new physics. A search for the CLFV decay $\mu^+ \to e^+\gamma$ by the MEG collaboration (see [3] and references therein for a detailed report of the experiment motivation, design criteria and goals) has been done at the Paul Scherrer Institut (PSI) in Switzerland in the period 2008-2013. Preliminary results [4,5,6] set a limit on the branching ratio of this decay $\mathcal{B} < 5.7 \times 10^{-13}$ at 90% C.L.

Figure 1 shows a schematic of the MEG apparatus, having at the core a magnetic spectrometer with a thin target at the centre, where a beam of positive muons stop and decay.

The signal consists of a positron and a γ–ray back to back each with energy of 52.83 MeV (half of the muon mass) and with a common origin in time and space.

The positron is tracked in a high intensity magnetic field by a set of low-mass drift chambers measuring its trajectory, followed by a scintillator based timing counter measuring its emission time. The γ–ray is measured by a liquid xenon homogeneous calorimeter located outside the magnet covering the angular region opposite to the spectrometer. The acceptance of the detector for the signal is ~ 11%.

The signal can be mimicked by various processes: Michel ($\mu^+ \to e^+\nu\bar{\nu}$) and radiative muon decays (RMD) ($\mu^+ \to e^+\gamma\nu\bar{\nu}$), Bremsstrahlung and positron annihilation-in-flight (AIF) ($e^+e^- \to \gamma\gamma$). Accidental coincidences between a positron and a γ-ray from different processes close in energy to their kinematic limits with direction and timing coincident within the detector resolution are the dominant source of background.

The rate of accidental coincidences is proportional to the square of the μ^+ decay rate, while the rate of signals is linearly proportional, the signal to background ratio is optimized with direct-current beams rather than pulsed beams. Hence the high intensity PSI continuous surface muon beam (see Sect. 2.1) is the ideal facility for such a search.

In the following, we present a detailed description of the analysis of the MEG full dataset in search for the $\mu^+ \to e^+\gamma$ decay. After a brief introduction to the detector and to the data acquisition system (Sect.2), the reconstruction algorithms are presented in detail (Sect.3), followed by a presentation of the event selection procedure and an in-depth discussion of the analysis (Sect.4). Finally, in the conclusions, some prospects for future improvements are outlined (Sect.5).

2 The MEG detector

Editor's comments:
Section coordinator: Paolo Walter Cattaneo
Text: 5.
Figure: 5.

In the following the MEG detector is briefly presented, emphasising the aspects relevant for the analysis, a detailed description is available in [7].

In this paper, we adopt a cylindrical coordinate system (r, ϕ, z) with origin in the centre of the magnet (see Fig.1). The z-axis is parallel to the magnet axis and directed along the incoming muon beam. The axis defining $\phi = 90$ (the y-axis of the corresponding Cartesian coordinate system) is directed upwards and, as a consequence, the x-axis is directed opposite to the centre of the xenon calorimeter.

Positrons move along trajectories of decreasing ϕ coordinate. When required, the polar angle θ with respect to the z-axis is also used. The region with $z < 0$ is referred as upstream, that with $z > 0$ as downstream.

2.1 Beam

The beam requirements are governed by the need for a high intensity, small emittance, almost monochromatic source of stopped positive muons at the centre of the detector, with minimal background from other sources. These goals are met by the πE5 channel at PSI, in combination with the MEG beam line, providing one of the world's highest intensity continuous muon beams, capable of delivering more than 10^8 μ^+/s. These surface muons of momentum 28 MeV/c, close to the kinematic edge and corresponding to the peak of the momentum distribution of stopped π^+-decay at the surface of the production target, are selected within a momentum-byte of 5–7%. The final intensity is tuned to a stopping rate on the target of 3×10^7 μ^+/s to match the rate capabilities of the tracking system and hence to achieve the optimal sensitivity of the experiment. The eight times higher beam related background due to positrons in the initial beam channel is efficiently removed by a combination of Wien filter and collimator system, while the muon stopping distribution at the target is optimised by a degrader system comprising of a 300 μm thick Mylar® foil and the He-Air atmosphere inside the spectrometer in front of the target. The final round Gaussian beam-spot profile corresponds to $\sigma_{x,y} \approx 10$ mm. Furthermore, both a negative pion beam tune of 70.5 MeV/c

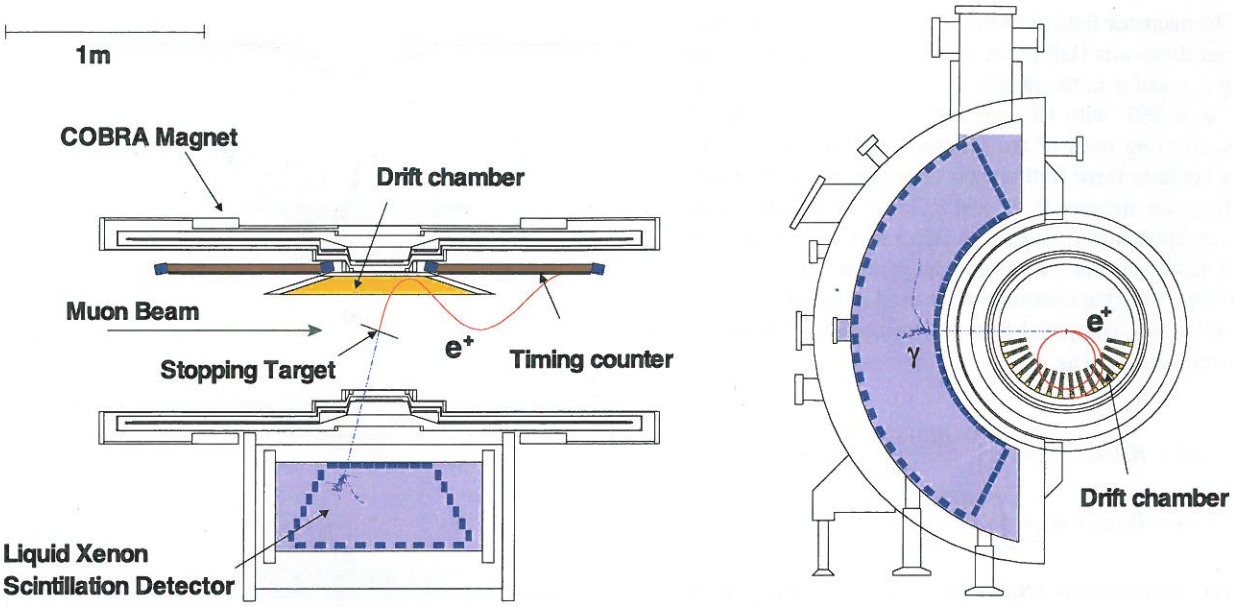

Figure 1 Schematic view of the MEG detector showing one simulated signal event emitted from the target.

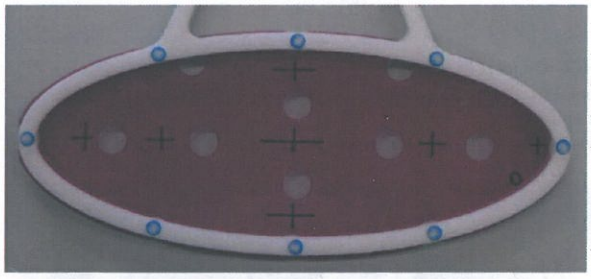

Figure 2 The muon stopping target mounted in a Rohacell frame.

used to produce monochromatic γ-rays via the pion charge exchange process and a 53 MeV/c positron beam tune to produce Mott scattered positrons close to the energy of the positron in a $\mu^+ \to e^+\gamma$ decay, are used for detector calibration purposes (Sect. 2.7).

2.2 Target

Positive muons are stopped in a thin target at the centre of the spectrometer, where they decay at rest. The target is required to have a stopping efficiency higher than 80%, while multiple scattering, Bremsstrahlung and annihilation-in-flight of positrons from muon decays inside the target should be minimised. These opposing requirements are satisfied by using a 205 μm thick layer of polyethylene and polyester (density 0.895 g/cm^3) with an elliptical shape with semi-major and semi-minor axes of 10 cm and 4 cm, respectively. The target foil is outfitted with seven cross marks and eight holes of radius 0.5 cm to allow for optical survey and software alignment. The foil is mounted in a Rohacell frame, which is attached to the tracking system support frame, and positioned such that the θ angle of the direction perpendicular to the target is $\sim 70°$. A picture of the target before installation in the detector is shown in Fig. 2.

2.3 The COBRA magnet

The COBRA (COnstant Bending RAdius) magnet [8] is a thin-wall superconducting magnet generating a gradient magnetic field, ranging from 1.27 T at the centre to 0.49 T at either end of the magnet cryostat. This is at variance with a uniform solenoidal field where positrons emitted transversely are confined in the spectrometer. It allows stable operation of the positron spectrometer in a high-rate environment. The gradient magnetic field is specially designed so that the positrons emitted from the target follow a trajectory with an almost constant projected bending radius weakly dependent on the emission polar angle θ (Fig. 3(a)). Only high-momentum positrons can therefore reach the tracking system placed at the outer radius of the inner bore of COBRA. Another important feature of this configuration is that the positrons emitted at $\cos\theta \sim 0$ are rapidly removed (Fig. 3(b)).

The central part of the superconducting magnet is as thin as $0.197\,X_0$ so that only a small fraction of the γ-rays from the muon decays on the target interact before reaching the LXe detector placed outside COBRA. The COBRA magnet is equipped with a pair of compensation coils to reduce the stray field around the LXe detector for the operation of the photomultiplier tubes (PMTs).

The magnetic field of COBRA was measured with a commercial three-axis Hall probe mounted on a wagon moving along z, r and ϕ in the ranges $|z| < 110\,\text{cm}$ with 111 steps, $0° < \phi < 360°$ with 12 steps and $0 < r < 29\,\text{cm}$ with 17 steps, covering most of the positron tracking volume. The probe contains three Hall sensors orthogonally aligned such that they can measure B_z, B_r and B_ϕ individually. Due to the main component B_z being much larger than the others, even small misalignments could cause large errors on B_r and B_ϕ. Therefore, only the measured B_z is used in the analysis and B_r and B_ϕ are computed from the measured B_z using the Maxwell equations as

$$B_\phi(z,r,\phi) = B_\phi(z_0,r,\phi) + \frac{1}{r}\int_{z_0}^{z} \frac{\partial B_z(z',r,\phi)}{\partial \phi} dz'$$

$$B_r(z,r,\phi) = B_r(z_0,r,\phi) + \int_{z_0}^{z} \frac{\partial B_z(z',r,\phi)}{\partial r} dz'.$$

The computations require the measured values for B_r and B_ϕ only at the plane defined by $z = z_0$. This plane is chosen at $z_0 = 1\,\text{mm}$ near the symmetry plane at the magnet centre where B_r is measured to be small ($|B_r| < 2 \times 10^{-3}$ T) as expected. The effect of the misalignment of the B_ϕ-measuring sensor on $B_\phi(z_0,r,\phi)$ is estimated by requiring the reconstructed B_r and B_ϕ be consistent with the other Maxwell equations.

The continuous magnetic field map used in the analysis is obtained by interpolating the measurements of the magnetic field at the grid points by a B-spline fit [9].

2.4 The Drift Chamber system

The Drift CHamber (DCH) system [7,10] is designed to ensure precision measurement of the trajectory and momentum of the positrons from $\mu^+ \to e^+\gamma$ decays. It must fulfil several stringent requirements: cope with a huge number of positrons from Michel decays from μ^+ in the target, be a low-mass tracker, as the momentum resolution is limited by multiple Coulomb scattering and in order to minimise the accidental γ-ray background by positron AIF, and finally provide excellent resolution in the measurement of the radial as well as of the longitudinal coordinate.

The DCH system consists of 16 identical independent modules, placed inside COBRA and aligned in a half circle with 10.5° intervals covering the azimuthal region between 191.25° and 348.75° and the radial region between 19.3 cm and 27.9 cm (see Fig. 4)

Each module has a trapezoidal shape with base lengths of 40 cm and 104 cm, without any supporting structure on the long side to reduce the amount of material. The modules are mounted with the long side in the inner part of the spectrometer (small radius) and the short one positioned on the central coil of the magnet (large radius) (for a sketch see Fig. 1).

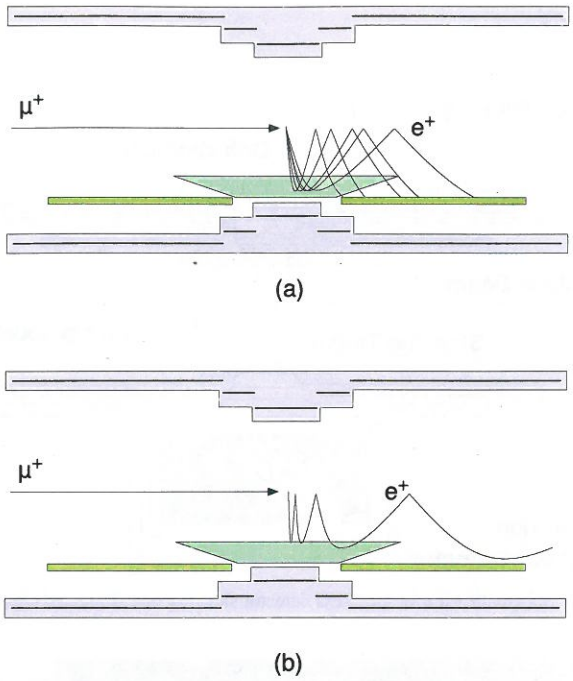

Figure 3 Concept of the gradient magnetic field of COBRA. The positrons follow trajectories at constant bending radius weakly dependent on the emission angle θ (a) and those transversely emitted from the target ($\cos\theta \sim 0$) are quickly swept away from the central region (b).

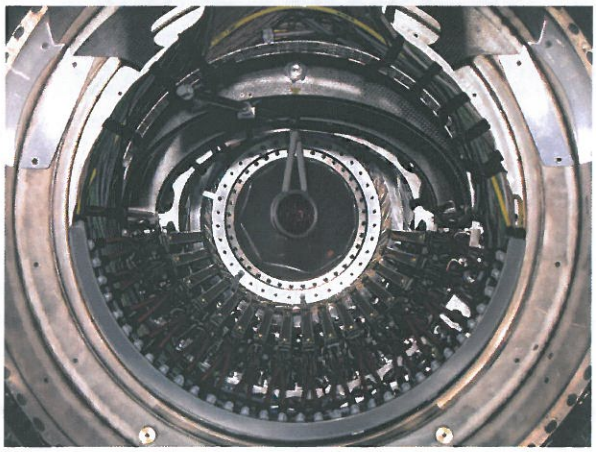

Figure 4 View of the DCH system from the downstream side of the MEG detector. The muon stopping target is placed in the centre, the 16 DCH chamber modules are mounted in a half circle.

Each module consists of two detector planes operated independently. Each plane consists of two cathode foils (12.5 μm-thick aluminised polyamide) with a 7 mm wide gap filled with a gas mixture He:C_2H_6 = 50:50. In between the foils there is a wire array containing alternating anode and po-

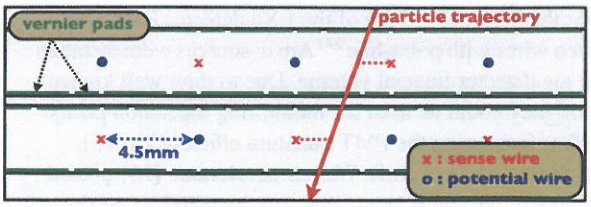

Figure 5 Schematic view of the cell structure of a DCH plane.

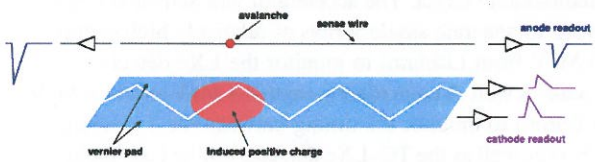

Figure 6 Schematic view of the Vernier pad method.

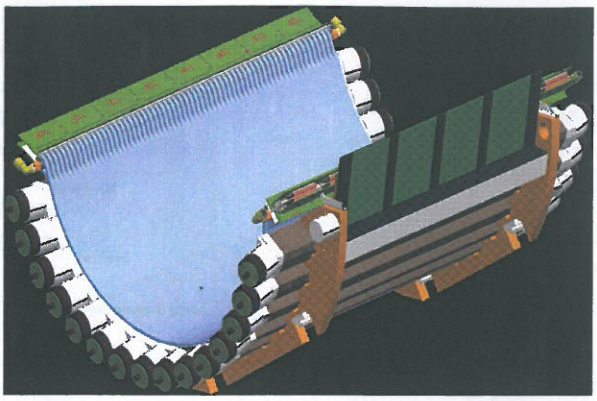

Figure 7 Schematic picture of a TC sector. Scintillator bars are read out by PMTs.

tential wires, stretched in the axial direction and mounted with a pitch of 4.5 mm with an anode-cathode distance of 3.5 mm. The two planes are separated by a gap of 3 mm. The two wire arrays in the same module are staggered in radial direction by half a drift cell to resolve left-right ambiguities (see Fig. 5). On the cathode foils, both inner and outer, a double wedge pad structure is etched with Vernier cycle $\lambda = 5$ cm as depicted in Fig. 6. The signals induced on the upper and lower pads depend on the hit position inside the Vernier cycle and allow the precise determination of the longitudinal coordinate.

Thanks to such a low-mass construction and the use of a helium-based gas mixture, the average amount of material in a DCH module sums up to only 2.6×10^{-4} X_0, which totals 2.0×10^{-3} X_0, in average, along the positron track.

2.5 The Timing Counter

The Timing Counter (TC) is dedicated to measure precisely the impact time of positrons to infer their emission time at the decay vertex in the target by correcting for the track length obtained from the DCH information.

The main requirements of the TC are:

- fast response to be used in the online trigger algorithms and to avoid rate effects;
- fast and approximate (~ 5 cm) positron impact point position resolution for online trigger;
- excellent (~ 50 ps) positron impact point time resolution;
- good (~ 1 cm) positron impact point position resolution in the offline event analysis;
- reliable operation in a harsh environment: high and non-uniform magnetic field, possibility of ageing effects, high rate;
- cover the full acceptance region for signal while matching the tight mechanical constraints dictated by the DCH system and COBRA;

these goals were achieved through extensive laboratory and beam tests [11,12,13].

As apparent from Fig. 1, the TC matches the signal kinematics and is compatible with the mechanical constraints by the placement of one module (sector) upstream and the other downstream.

Each sector (see Fig. 7 for a sketch) is barrel shaped with full angular coverage for positrons from $\mu^+ \to e^+\gamma$ decays having the γ-ray points to the LXe detector and consists of an array of 15 scintillating bars with 10.5° gap between adjacent bars. Each bar has an approximate square section and size $4.0 \times 4.0 \times 79.6$ cm^3 and is read out by a couple of fine-mesh 2" PMTs for high magnetic fields coupled at the ends with optical grease.

The inner radius of a sector is 29.5 cm, such that only positrons with momentum close to the kinematic limit hit the TC.

2.6 LXe detector

The MEG γ-ray detector [14] requires excellent position, time and energy resolutions to minimise the number of accidental coincidences between background γ-rays and positrons, which are the dominant background process (see Sect.4.3.2).

It consists of a homogeneous calorimeter able to fully contain the shower induced by a 52.83 MeV γ-ray with capability of measuring the first interaction point, the interaction time and the energy deposit. That allows a γ-ray high detection efficiency with the drawback of not measuring directly the γ-ray direction.

Liquid Xenon (LXe), with its high density (and short radiation length) is an efficient detector medium for γ-rays,

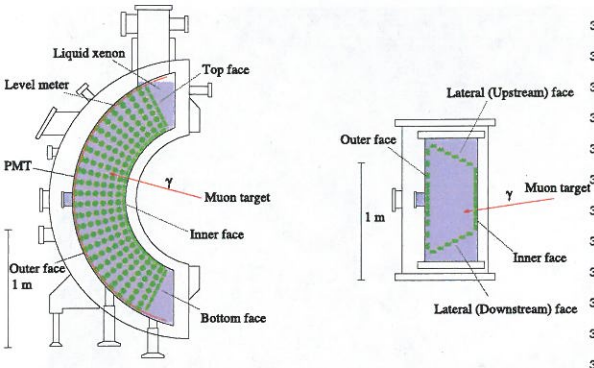

Figure 8 Schematic view of the LXe detector: from the side (left), from the top (right).

which can rely both on ionisation charges and on scintillation photons. In MEG, only the scintillation photons are used to guarantee a prompt response of the detector.

A schematic view of the LXe detector is shown in Fig. 8 with its C-shaped structure fitting the outer radius of COBRA. The fiducial volume is ~ 800 ℓ, covering 11% of the solid angle viewed from the centre of the stopping target; it is read out by 846 PMTs submerged directly in LXe to detect the scintillation photons. They are placed on all six faces of the detector (inner, outer, upstream, downstream, top and bottom), with different PMT densities. The detector's depth is 38.5 cm, corresponding to ~ 14 X_0 and fully containing showers induced by 52.83 MeV γ-rays.

2.7 Calibration

Redundant calibration and monitoring tools were devised and integrated in the experiment in order to constantly check the operation of single sub-detectors (*e.g.* photodetector equalisation, inter-bar timing, energy scale, etc.) and multiple detectors simultaneously (relative timing etc.).

Some of the monitoring and calibrations could be performed during normal data taking, making use of particles coming from muon decays: the end points of both positron and γ-ray spectra to check the energy scale or the radiative muon decays to check the LXe–TC relative timing. Additional calibrations required the installation and usage of new tools, devices and detectors [7]. A list of some of these methods is presented in Table 1 and are briefly discussed below.

It is important to calibrate and monitor the PMT gains of the LXe detector in a reliable and stable way. PMT gains are estimated by using 44 blue LEDs immersed in the LXe at different positions. Dedicated runs for gain measurements in which LEDs are flashed at different intensities are taken every two days. In order to monitor the PMT long-term instabilities, constantly flashing LED data have been taken during physics runs.

For the inter-calibration of the LXe detector PMTs, thin tungsten wires with point-like ^{241}Am α-sources were installed inside the detector fiducial volume. Due to their well known position they could be used for monitoring the xenon purity as well as measuring the PMT quantum efficiencies [15].

A dedicated Cockcroft–Walton accelerator [16] placed downstream the muon beam line was installed to produce γ-rays of known energy by shooting MeV protons on a lithium tethraborate target. The accelerator was activated twice per week to generate single γ-rays of relatively high energy (17.6 MeV from Lithium) to monitor the LXe detector energy scale as well as coincident γ-rays (4.4 MeV and 11.6 MeV from Boron) to monitor the timing between the TC scintillator bars as well as the TC–LXe detector timing (see Table 1 for the relevant reactions).

Once per year a dedicated calibration run was performed by shooting negative pions on a liquid hydrogen target placed at the centre of COBRA. Coincident γ-rays from π^0 decays produced in the charge exchange reaction $\pi^- p \to \pi^0 n$ (CEX) and detected simultaneously by the LXe detector and a dedicated BGO crystal detector are used to measure the response of the LXe detector at 55 MeV (and 83 MeV), which is close to the $\mu^+ \to e^+\gamma$ signal region.

A low-energy calibration point is provided by 4.4 MeV γ-rays from an ^{241}Am/Be source that is moved periodically in front of the LXe detector during beam-off periods.

A neutron generator exploiting the reaction in Table 1 is the only method combining data acquired under different beam conditions, in particular those acquired during the normal MEG condition and the CEX condition.

Mott scattered positrons are also yearly acquired to monitor and calibrate the Spectrometer with all the benefits associated with the usage of a quasi monochromatic energy line at 53 MeV [17].

2.8 Front-end electronics

One of the most innovative approach of MEG is the use of a high frequency digitisers based on the Switched Capacitor Array technique, called Domino Ring Sampler 4 (DRS4) [18], for all ~ 3000 readout channels. It was custom designed for MEG with the goal of storing a waveform of 1024 samples for each channel having a signal above threshold. The sampling rate is 1.6 GHz for TC and LXe, which perform high resolution timing measurements, and 0.8 GHz for DCH, which has less stringent timing requirements.

Each waveform is processed offline applying e.g. baseline subtraction, spectral analysis, noise filtering, digital constant fraction discrimination etc. such as to optimise the extraction of the variables relevant for the measurement. This approach gives the opportunity of reprocessing the full waveform information offline with improved algorithms to optimise the performances of the detector.

Table 1 The calibration tools of the MEG experiment.

	Process	Energy	Main Purpose	Frequency
Cosmic rays	$\mu^{\pm}$ from atmospheric showers	Wide spectrum O(GeV)	LXe-DCH relative position	daily
			DCH alignment	
			TC energy and time offset calibration	
Charge exchange	$\pi^- p \to \pi^0 n$ $\pi^0 \to \gamma\gamma$	55, 83, 129 MeV γ-rays	LXe energy scale/resolution	yearly / monthly
Radiative μ–decay	$\mu^+ \to e^+\gamma\nu\bar{\nu}$	52.83 MeV endpoint γ-rays	LXe energy scale	weekly
			LXe-TC relative timing	
Normal μ–decay	$\mu^+ \to e^+\nu\bar{\nu}$	52.83 MeV endpoint positrons	DCH energy	daily
Mott positrons	e^+target $\to e^+$target	~ 50 MeV positrons	DCH energy	yearly / monthly
Proton accelerator	^{7}Li$(p,\gamma_{17.6})^8$Be	14.8, 17.6 MeV γ-rays	LXe energy scale/purity	weekly
	^{11}B$(p,\gamma_{16.1})^{12}$C	4.4, 11.6, 16.1 MeV	TC interbar/ LXe–TC timing	weekly
Neutron generator	^{58}Ni$(n,\gamma_9)^{59}$Ni	9 MeV γ-rays	LXe energy scale	daily
Radioactive source	^{241}Am	5.5 MeV α	LXe energy scale	daily
Radioactive source	^{9}Be$(\alpha_{^{241}Am}, n)^{12}C_\star$ ^{12}C$_\star \to ^{12}$C$\gamma_{4.4}$	4.4 MeV γ-rays	LXe PMT intercalibration	daily

2.9 Trigger

An experiment to search for ultra-rare events in a huge background due to high decay rate needs a quick and efficient event selection, which demands the combined use of high-resolution detection techniques with fast front-end, digitising electronics and trigger. The trigger system plays an essential role in processing the detector signals to find the signature of $\mu^+ \to e^+\gamma$ events in a high-background environment [19,20]. The trigger must strike a compromise between a high efficiency for signal, high live time and very high background rejection rate. The trigger rate should be kept below 10 Hz so as not to overload the data acquisition (DAQ) system.

The set of observables to be reconstructed at trigger level includes:

- the γ-ray energy;
- the relative e^+–γ direction;
- the relative e^+–γ timing.

The stringent limit due to latency of the readout electronics prevents using any information from the DCH: the electron drift time toward the anode wires being too long. Therefore a reconstruction of the positron momentum cannot be obtained at the trigger level even if the requirement of a TC hit is equivalent to the requirement of positron momentum $\gtrsim$ 45 MeV. The γ-ray energy is the most important observable to be reconstructed, due to the steep decrease of the spectrum at the end-point. For this reason the calibration factors for the PMT signals of the LXe detector (such as PMT gains and quantum efficiencies) are continuously monitored and periodically updated. The energy deposited in the LXe detector is estimated by the linear sum of the PMT pulse amplitudes.

The amplitudes of the inner-face PMT pulses are also sent to comparator stages to extract the index of the PMT collecting the highest charge, which provides a robust estimator of the interaction vertex of the γ-ray in the LXe detector. This vertex and the target centre provides an estimate of the γ-ray direction.

On the positron side, the coordinates of the TC interaction point are the only information available online. The radial coordinate is given simply by the radial location of the TC, while, thanks to its segmentation along ϕ, this coordinate is identified with the bar index of the first hit (first bar encountered moving along the positron trajectory). The local z coordinate on the hit bar is measured by the ratio of charges on the PMTs on opposite sides of the bar with a resolution ~ 5 cm.

Under the assumption of the momentum being that of the signal and the direction opposite to that of the γ-ray, by means of Monte Carlo (MC) simulations, each PMT index is associated with a region of the TC. If the online TC coordinates fall into this region, the relative e^+–γ direction is compatible with the back-to-back condition.

The interaction time of the γ-ray in the LXe detector is extracted by a fit of the leading edge of PMT pulses with a ~ 2 ns resolution. The same procedure allows to estimate the time of the positron hit on the TC with a comparable resolution. The relative time is obtained from their difference; fluctuations due to the time-of-flight of each particle are within the resolutions.

2.10 DAQ System

Editor's comments:
Section coordinator: Luca G., Stefan R.

Text: 0.5
Figure: 1.

The DAQ challenge is to perform the readout of the whole detector waveforms maintaining the system efficiency, defined as the product of the online efficiency (ε_{trg}) and the DAQ live time fraction (LT), as high as possible.

At the beginning of data taking, with the help of MC simulations, the trigger configuration that maximised the DAQ efficiency was found to have $\varepsilon_{trg} \approx 90\%$ and LT $\approx 85\%$ and an associated event rate $R_{daq} \approx 7$ Hz, almost seven orders of magnitude lower than the muon stopping rate.

The bottleneck was found in the waveform readout time from the VME boards to the offline disks, lasting as much $t_{ro} \approx 24$ ms/event; the irreducible contribution to the dead time is the DRS4 read out time and accounts for 625 μs. This limitation has been overcome starting from the 2011 run thanks to a multiple buffer read out scheme, in our case three buffers. In this scheme, during the event readout from a buffer, in case of a new trigger, new waveforms can be written in the following one; the system experiences dead time only when there are no empty buffers left. This happens when three events occur within a time interval equal to the read out time t_{ro}. The associated live time is

$$LT = e^{-R_{daq} \cdot t_{ro}} \cdot [1 + R_{daq} \cdot t_{ro} + (R_{daq} \cdot t_{ro})^2/2!],$$

and is $\geq 99\%$ for event rate up to ~13 Hz.

The multiple buffer scheme allowed to relax the trigger conditions, in particular for what concerns the relative e^+–γ direction, leading to a much more efficient DAQ system, from 75% in 2009-2010 to 97% in the 2011-2013 period. Figure 9 shows the two described working points, the first part refers to 2009 and 2010 runs, while the second one from 2011 to 2013.

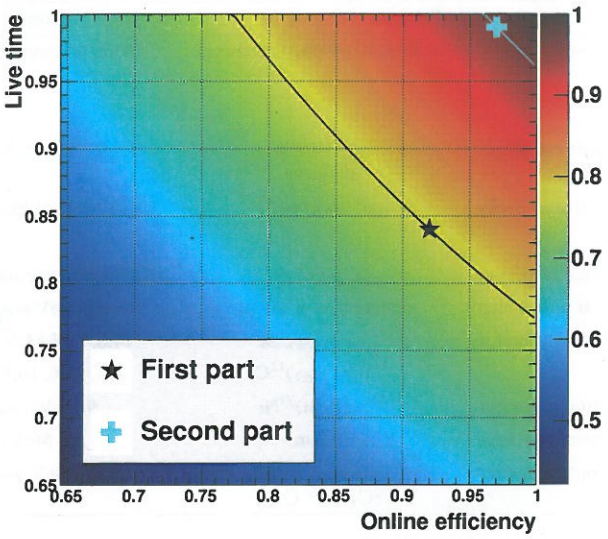

Figure 9 Contour lines for DAQ efficiency during different run periods: without (First part) and with (Second part) the multiple buffer read out scheme.

3 Reconstruction

Editor's comments:
Section coordinator: Toshiyuki Iwamoto
Text: 5.5
Figure: 12.

In this section the reconstruction of high-level objects is presented. More information about low-level objects (e.g. waveform analysis, hit reconstruction) and calibration issues are available in [7].

3.1 γ-ray reconstruction

Editor's comments:
Section coordinator: Toshiyuki, Ryu, Yusuke
Text: 1.5
Figure: 2.

A 52.83 MeV γ-ray interacts with LXe predominantly via the pair production process, followed by an electromagnetic shower. The major uncertainty in the reconstruction stems from the event-by-event fluctuation in the shower development. A series of algorithms were developed to provide the best estimates of the energy, the first interaction position and time of the incident γ-ray while identifying and eliminating pile-ups.

For reconstruction inside the LXe detector, a special coordinate system (u, v, w) is used: u coincides with z in the MEG coordinate system; v is directed along the negative ϕ-direction at the radius of the fiducial volume inner face (r_{in} = 67.85 cm); $w = r - r_{in}$, measures the depth from r_{in}. The fiducial volume of the LXe detector is defined as $|u| < 25$ cm, $|v| < 71$ cm, and $0 < w < 38.5$ cm ($|\cos\theta| < 0.342$ and 120° in ϕ) in order to ensure high resolutions, especially for energy and position measurements.

The reconstruction starts with waveform analysis extracting charge and time from the PMT waveforms. The digital-constant-fraction method is used to determine an (almost) amplitude independent pulse time, defined as the time when the signal reaches a predefined fraction (20%) of the maximum pulse height. To maximise the signal-to-noise ratio for the determination of the charge, a digital high-pass filter[1] with a cutoff frequency of ~ 10 MHz, is applied.

[1] The high-pass filter is written:

$$y[i] = x[i] - \frac{1}{M}\sum_{j=1}^{M} x[i - M + j],$$

The charge is converted to the number of photoelectrons (N_{pe}) and to the number of scintillation photons impinging on the PMT (N_{pho}) as follows:

$$N_{\mathrm{pe},i} = Q_i/eG_i(t),$$
$$N_{\mathrm{pho},i} = N_{\mathrm{pe},i}/\mathcal{E}_i(t),$$

where $G_i(t)$ is the PMT gain and $\mathcal{E}_i(t)$ is the product of the quantum efficiency and collection efficiency. These quantities vary over time[2] and, thus, were continuously monitored and calibrated using the calibration sources instrumented in the LXe detector.

The PMT gain is computed using blue LEDs, flashed at different intensities, from the statistical relation between the mean and variance of the observed charge,

$$\sigma^2_{Q_i} = eG_i\bar{Q}_i + \sigma^2_{\mathrm{noise}},$$

and the time variation is followed by using the LED events constantly flashed (1 Hz) during the physics data taking.

The product of the quantum efficiency and collection efficiency, $\mathcal{E}_i(t)$, is evaluated using the α events from the ^{241}Am source and the Li 17.6-MeV γ-line produced with the Cockcroft–Walton accelerator by comparing the observed photoelectrons with the expected number of scintillation photons evaluated with the MC simulation,

$$\mathcal{E}_i = \bar{N}_{\mathrm{pe},i}/\bar{N}^{\mathrm{MC}}_{\mathrm{pho},i}.$$

This calibration was performed two or three times per week to monitor the time dependence.

3.1.1 γ-ray position

The 3D position of the γ-ray conversion point is determined by a χ^2-fit of the distribution of scintillation photons, calculated from the solid angle subtended by each PMT photocathode, to the observed N_{pho} distribution. To minimise the effect of shower fluctuation, a limited number of PMTs on the inner face is used in the fit; PMTs inside a radius of 3.5-PMT distance from the initial estimation by the weighted mean around the maximum output PMT are used. For events resulting in $w < 12$ cm, the fit is repeated with a further reduced number of PMTs, inside a radius of 2-PMT distance from the first fit result. The remaining bias on the result, due to the inclined incidence of the γ-ray onto the inner face, is corrected using results from the MC simulation.

The performance of the position reconstruction is evaluated by the MC simulation and it is validated in dedicated CEX experiments by placing lead collimators in front of the LXe detector. The average position resolutions along the two orthogonal inner-face coordinates (u, v) and the depth direction (w) are estimated to be ~ 5 and ~ 6 mm, respectively.

The reconstructed position is given in the detector local coordinate system and the conversion to the MEG coordinate system relies on the alignment of the LXe detector with the rest of the MEG detector. The LXe detector position was precisely surveyed relative to the MEG coordinate system by a laser tracker. After the thermal shrink of the cryostat and the PMT support structures at LXe temperature are taken into account, the PMT positions are extracted based on the above information. The final alignment of the detector with respect to the positron spectrometer is described in Sect. 3.3.1.

3.1.2 γ-ray timing

The determination of the γ-ray emission time from the target t_γ starts from the determination of the arrival time of the scintillation photons on each PMT $t^{\mathrm{PMT}}_{\gamma,i}$ as described in Sect. 3.1. To relate this time to the γ-ray conversion time, the propagation time of the scintillation photons must be subtracted as well as any hardware-induced time offset (e.g. cable length).

The propagation time of the scintillation photons is evaluated as a function of the distance and incident angle from the reconstructed conversion point to the PMT. The former contribution is calculated using an effective light velocity of ~ 8 cm/ns, a value empirically determined by fitting our measurement data. The latter comes from the fact that the fraction of indirect (scattered or reflected) scintillation photons increases with larger incident angle. An empirical function was found and calibrated using the $\pi^0 \to \gamma\gamma$ events produced in CEX runs in which the time of one of the γ-rays is measured by two plastic scintillator counters with a lead shower converter as a reference time. Once the propagation time is subtracted, the remaining time offset can be extracted from the same $\pi^0 \to \gamma\gamma$ events for each PMT by comparing the PMT hit time with the reference time.

After the subtraction of these effects, the γ-ray conversion time (t^{LXe}_γ) is obtained by combining the timings of those PMTs ($t^{\mathrm{PMT}}_{\gamma,i}$) which observe more than 50 N_{pe} and are not in the shadow of the walls to minimise

$$\chi^2 = \sum_i \frac{(t^{\mathrm{PMT}}_{\gamma,i} - t^{\mathrm{LXe}}_\gamma)^2}{(\sigma^{1\text{-PMT}}_{t_\gamma}(N_{\mathrm{pe},i}))^2}.$$

The single-PMT time resolution is measured in the CEX runs to be $\sigma^{1\text{-PMT}}_{t_\gamma}(N_{\mathrm{pe}} = 500) = 400$–$540$ ps, depending on the location of the PMT, and nearly proportional to $1/\sqrt{N_{\mathrm{pe}}}$. Typically 150 PMTs, ~70 000 N_{pe} in total, are used to reconstruct 50-MeV γ-rays. The PMTs with large contributions to

where $x[]$ is the input signal, $y[]$ is the output signal, and $M = 105$ is the number of points used in the average. This filter is based on the moving average, which has a good response in time domain with a simple and fast algorithm.

[2] Two kinds of instability in the PMT response were observed: one is a long-term gain decrease considered to be due to the fatigue of the dynodes and the other is a rate-dependent gain shift considered to be due to the charge buildup on the dynodes.

χ^2 are rejected during this fitting procedure to remove pile-up effects.

Finally, the γ-ray emission time from the target t_γ is obtained by subtracting the time-of-flight between the positron reconstructed vertex on the target and the reconstructed conversion point in the LXe detector from t_γ^{LXe}.

The timing resolution σ_{t_γ} is evaluated by looking at the time difference between the two γ-rays from π^0 decay after the subtraction of the contributions due to the uncertainty of the π^0 decay position and to the timing resolutions of the reference counters. From measurements at 55 and 83 MeV, the energy dependence was estimated and corrected, resulting in $\sigma_{t_\gamma}(E_\gamma = 52.83\ \mathrm{MeV}) \sim 64$ ps.

3.1.3 γ-ray energy

The reconstruction of the γ-ray energy E_γ is based on the total sum of scintillation photons collected by the PMTs. A summed waveform with the following coefficients over all the PMTs is formed and the energy is determined by integrating it:

$$F_i = \frac{A_i \cdot W_i(u,v,w)}{eG_i(t) \cdot \mathcal{E}_i(t)} \cdot \Omega(u,v,w) \cdot U(u,v,w) \cdot H(t) \cdot S,$$

where A_i is a correction factor for the geometrical coverage, which is dependent on the PMT location[3]; $W_i(u,v,w)$ is a weighting factor for the PMT; $\Omega(u,v,w)$ is a correction factor for the solid angle subtended by photo-cathodes at the conversion point, applied only for shallow events ($w < 3$ cm) for which the light collection efficiency is very sensitive to the relative position of each PMT and the conversion point; $U(u,v,w)$ is a position-dependent non-uniformity correction factor determined by the responses to the 17.6- and 55-MeV γ-rays; $H(t)$ is a correction factor for the time-varying LXe scintillation light yield; and S is a constant conversion factor of the energy scale determined by the 55- and 83-MeV γ-rays with a precision of 0.3%. The weighting factor $W_i(u,v,w)$ is common to the PMTs on the same face and determined by minimising the resolution in response to 55-MeV γ-rays.

It is important to recognise and unfold pile-up γ-rays in order to suppress high energy γ-ray background as well as to avoid a loss of signal efficiency because around 15% of triggered events suffer from pile-up at the nominal beam rate. The pile-up signature is identified by the following three methods.

The first method identifies multiple γ-rays with different timings using the χ^2/NDF value in the time fit. In contrast to the time reconstruction, all the PMTs observing more than 50 N_{pe}, including PMTs in the shadow and those with large contribution to χ^2, are used to identify pile-up events.

[3]The coverage on the outer face is, for example, 2.6 times less dense than that on the inner face

The second method identifies pile-up events in different positions by searching for the photon distribution on the inner and outer faces for spatially separated peaks. If the event has two or more peaks and they are indissociable in the third method below, a pile-up removal algorithm is applied to the PMT charge distribution. A position-dependent table containing the average charge of each PMT in response to 17.6-MeV γ-rays is prepared beforehand. Once a pile-up event is identified, the energy of the event is estimated by fitting the PMT charges to the table without using PMTs around the secondary γ-ray. Then, the PMT charges around the secondary γ-ray are replaced with the charges estimated by the fit. Finally, the energy is reconstructed as a sum of the individual PMT charges with the coefficients F_i, instead of integrating the summed waveform.

The third method identifies multiple γ-rays and unfolds them by combining the information from summed waveforms and the two methods above. First, the total sum waveform is searched for temporally separated pulses. Next, if the event is identified as a pile-up event by either of the two methods above, a summed waveform over PMTs near the secondary γ-ray is formed to search for multiple pulses. The pulse found in the partial sum waveform is added to the list of pulses if the time is more than 5 ns apart from the other pulse times. Then, a superimposition of N template waveforms is fitted to the total sum waveform, where N is the number of pulses detected in this event. Figure 10 shows an example of the fitting, where three pulses are detected. Finally, the contributions of pile-up γ-rays are subtracted and the remaining waveform is used for energy estimation.

The energy response of the LXe detector was studied in the CEX runs using π^0 decays with an opening angle between the two γ-rays >170°. The line shape is shown in Fig. 11 at two different conversion depth (w) regions. The line shape is asymmetric with a low energy tail mainly due to two reasons: the interaction of the γ-ray in the material in front of the LXe fiducial volume and the shower leakage from the inner face. The energy resolution is evaluated from the width of the line shape in the right-hand (high-energy) side (σ_{E_γ}) unfolding the finite width of the incident γ-ray energy distribution due to the imperfect back-to-back selection and a small correction for the different background conditions between the muon and pion beams. Since the response of the detector is dependent on the position of the γ-ray conversion, the fitted parameters of the line shape are functions of the 3D coordinates, mainly of w. The average resolution is measured to be $\sigma_{E_\gamma} = 2.3\%$ ($0 < w < 2$ cm, event fraction 42%) and 1.6% ($w > 2$ cm, 58%).

The energy resolutions and energy scale are cross-checked by fitting the background spectra measured in the muon decay data with the MC spectra folded with the detector resolutions.